A&A 405, 1025–1032 (2003)
DOI: 10.1051/0004-6361:20030672

Astronomy & Astrophysics

Angular momentum transport by internal gravity waves

I - Pop I main sequence stars

S. Talon[1,2] and C. Charbonnel[3,4]

[1] CERCA, 5160, boul. Décarie, suite 400, Montréal PQ H3X 2H9, Canada
[2] Département de Physique, Université de Montréal, Montréal PQ H3C 3J7, Canada
[3] Laboratoire d'Astrophysique de Toulouse, CNRS UMR 5572, OMP, 14, Av. E. Belin, 31400 Toulouse, France
[4] Observatoire de Genève, 51 ch. des Maillettes, 1290 Sauverny, Switzerland

Received 28 January 2003 / Accepted 16 April 2003

Abstract. We examine the generation of gravity waves by the surface convection zone of low-mass main sequence stars with solar metallicity. It is found that the total momentum luminosity in waves rises with stellar mass, up to the quasi-disappearance of the convection zone around 6500 K (corresponding to a mass of ~1.4 $M_\odot$ for solar metallicity) where the luminosity drastically drops. We calculate the net momentum extraction associated with these waves and explain how the calculated mass dependence helps resolve the enigma of the Li dip in terms of rotational mixing, forming a coherent picture of mixing in all main sequence stars.

Key words. hydrodynamics – stars: interiors – stars: late-type – stars: rotation – turbulence – stars: abundances

1. Clues to angular momentum transport in low-mass stars

In many locations of the Hertzsprung-Russell diagram, stars exhibit signatures of processes that require challenging modeling beyond the standard stellar theory[1]. In this context, rotation has become a major ingredient of modern models, especially when abundance anomalies have to be accounted for. In order to correctly describe the effects of rotation on stellar structure and evolution as well as on their "byproducts" like surface abundances or chemical yields, special emphasis has to be put on the evolution of the angular momentum distribution; this indeed is the feature that determines the extent and magnitude of rotation-induced mixing in stars.

In recent theoretical developments, the internal rotation law evolves as a result of contraction, expansion, meridional circulation, shear turbulence and mass loss; mixing of chemicals is directly linked to the rotation profile (see e.g. Talon 2003). The most sophisticated treatment of these hydrodynamical processes is based mainly on the work by Zahn (1992), Maeder (1995), Talon & Zahn (1997) and Maeder & Zahn (1998). It rests on only one assumption which is that the turbulence sustained by the shear is highly anisotropic. Two free parameters describe the magnitude of the horizontal shear and the erosion of the restoring force due to both the thermal and the mean molecular weight stratifications.

Such a self-consistent treatment has been successfully applied in various parts of the HR diagram. The strength of the theory is that the use of the same free parameters give very satisfactory results for stars over a large range of masses and evolutionary phases. For example, it explains the observed He and N enrichment in main sequence O-type and early B-type stars, in OB supergiants (e.g., Gies & Lambert 1992; Lennon et al. 1991; Herrero et al. 1999) and in A-type supergiants in the SMC (Venn 1999), as well as the B depletion in main sequence B-type stars (e.g., Venn et al. 1996); it also helps reproducing the number ratio of blue to red supergiants in the SMC (e.g., Meylan & Maeder 1982) and the observed WR/O ratios at solar metallicity. We refer to Maeder & Meynet (2000) for a more detailed description of the effects of rotation in massive stars and for relevant references.

In low-mass stars, the strongest observational constraints come from the so-called Li dip and from helioseismology. The Li dip is a characteristic feature of lithium abundances which is seen both in the field and in open clusters (e.g., Wallerstein et al. 1965; Boesgaard & Tripicco 1986; Balachandran 1995). It corresponds to a narrow region in effective temperature (around $T_{\rm eff} \sim$ 6650 K) where the surface Li abundances are reduced by up to ~2.5 dex. In the same region, low-mass stars are beginning to be spun down efficiently early on the main sequence (Boesgaard 1987), most probably via magnetic torquing.

Send offprint requests to: S. Talon,
e-mail: Suzanne.Talon@cerca.umontreal.ca

[1] By standard we refer to the modeling of non-rotating, non-magnetic stars, in which convection is the only large-scale mixing considered.

In modern rotating stellar models in which the transport of angular momentum and of chemicals by meridional circulation and shear turbulence is self-consistently taken into account, this leads to important lithium (and beryllium) destruction at the correct $T_{\rm eff}$ (Talon & Charbonnel 1998, hereafter TC98; Palacios et al. 2003, hereafter PTCF03). In addition rotation induced mixing inhibits the atomic diffusion in a way that explains the constancy of the CNO abundances within the Li dip (e.g., Varenne & Monier 1998; Takeda et al. 1998). Last but not least, these models do explain the evolution of Li surface abundances in evolved stars that originate from the hot side of the dip. It is worth recalling that all these results for low-mass stars on the blue side of the dip are obtained with the same values for the two above-mentioned parameters as those used in massive stellar models.

For still cooler main sequence stars however, the magnetic torque strengthens as the stellar convective envelope grows. If we assume here that all the momentum transport is assured by the wind-driven meridional circulation as it is on the blue side of the Li-dip, then too much lithium burning is obtained below $T_{\rm eff} \sim 6550$ K. Thus the rise of the Li abundance on the red side of the dip can be interpreted as the signature of another mechanism that efficiently transports angular momentum (but not chemicals) in lower mass stars (TC98). As a result, in these objects the magnitude of both meridional circulation and shear turbulence is reduced, as well as the Li depletion due to rotational mixing.

Such a mechanism is also required to shape the Sun's flat rotation profile (Chaboyer et al. 1995; Matias & Zahn 1998). At the solar age, models relying solely on turbulence and meridional circulation for momentum transport still predict large angular velocity gradients which are not present in the Sun.

Only two mechanisms have been proposed so far to transport angular momentum in addition to the classical hydrodynamical processes in order to enforce the flat rotation profile measured by helioseismology: magnetic fields (Charbonneau & MacGregor 1993; Barnes et al. 1999) and gravity waves (Schatzman 1993; Kumar & Quataert 1997; Zahn et al. 1997). As explained in TC98, in order to obtain a consistent picture of rotational mixing in all types of stars, the correct mechanism must become efficient in the center of the Li dip, namely at an effective temperature of ~6650 K.

While the original propositions for momentum extraction by gravity waves have received much criticism (Gough & McIntyre 1998; Ringot 1998), recent calculations performed by Talon et al. (2002, hereafter TKZ02) show that, through differential filtering, gravity waves are indeed able to extract momentum from the solar interior. Here we explore the same physics in the stellar mass range around the Li dip in order to verify whether it has the proper mass dependence as described by TC98 (see Fig. 1). Our goal is to present a coherent understanding of rotational mixing in *all* stars of the main sequence. We will firstly recall the main descriptions that have been made for wave excitation (Sect. 2) and explain how thermal dissipation of these waves leads to the formation of a filtering shear layer (Sect. 3). Results for momentum extraction by waves in stars of various masses are then presented (Sect. 4) and discussed (Sect. 5).

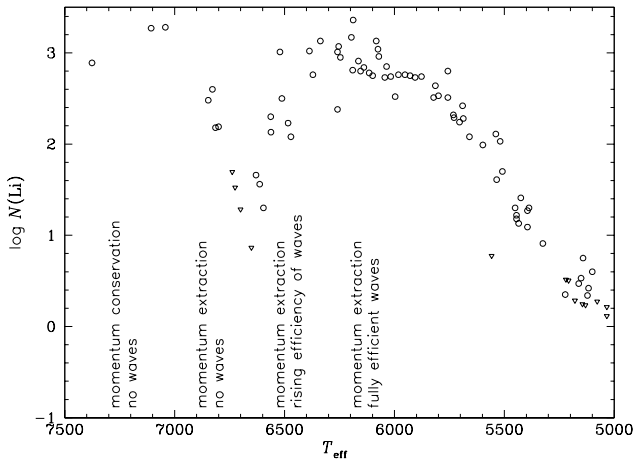

Fig. 1. Measured Li abundances in the Hyades. Superposed is the pattern of efficiency of momentum transport required to produce the Li gap via rotational mixing

2. Turbulent wave excitation

2.1. Two excitation mechanisms

The generation of gravity waves depends on the structure of the stellar convective envelope. On the main sequence, this region is rather large in solar mass stars (~30% in radius), while it shrinks as the stellar mass rises, representing only ~1% in a 1.45 $M_\odot$ star lying inside the Li dip. The characteristic convective frequency varies from $\nu_{\rm c} \sim 0.75\,\mu$Hz to $\nu_{\rm c} \sim 600\,\mu$Hz while the spherical harmonic number ℓ corresponding to the largest convective scale varies from $\ell_{\rm c} \sim 60$ to $\ell_{\rm c} \sim 1000$ in the same mass range. These variations are not smooth, rapid changes of convective properties occurring when $M_* \gtrsim 1.3\ M_\odot$. We wish to investigate how the wave spectrum produced by these convection zones varies as a function of stellar mass.

The exact properties of wave spectra remain somewhat uncertain. Excitation can be related to internal stresses that correlate with the mode's eigenfunction (Goldreich & Kumar 1990; Balmforth 1992; Goldreich et al. 1994). Gravity waves may also be excited by penetration below a convection zone, as observed in laboratory experiments (Townsend 1958) and in numerical simulations (Hurlburt et al. 1986, 1994; Nordlund et al. 1996; Kiraga et al. 2000). In a real star, both sources would contribute to wave generation and they are thus additive.

In this paper, we examine both sources, with emphasis not on their absolute values, but rather on their variation with stellar mass. Our computations are performed for stars between 1.1 and 1.45 $M_\odot$ with $Z = 0.02$ (see Table 1). We use the same code and input physics (eos, opacities, nuclear reactions) as in PTCF03. Wave characteristics are computed on the basis of ZAMS stellar structures. Note that in these objects the depth and structure of the convective envelope does not vary significantly over a main sequence lifetime (at least up to the age of the Hyades).

Table 1. Characteristics of the stellar models (with $Z = 0.02$) on the ZAMS and maximum frequency $\nu_{\max}$ used to capture the wave - mean flow interaction. ℓ_c is the largest convective scale, ν_c, the characteristic convective frequency and K_T, the thermal diffusivity.

M_* ($M_\odot$)	$T_{\rm eff}$ (K) zams	$T_{\rm eff}$ (K) Hyades	$\log(M_{zc}/M_*)$	ℓ_c	ν_c (μHz)	K_T (cm^2 s^{-1})	$\nu_{\max}$ (μHz)
1.1	5615	5640	−2.26	80	1.28	4.49×10^7	5.25
1.2	5905	5950	−3.09	117	3.30	4.49×10^8	5.25
1.3	6210	6260	−4.12	184	9.34	5.58×10^9	5.25
1.35	6370	6420	−4.92	269	22.8	3.06×10^{10}	10.5
1.4	6555	6595	−5.77	407	54.2	1.75×10^{11}	15.5
1.42	6620	6670	−6.44	599	114	5.47×10^{11}	15.5
1.43	6665	6710	−6.84	754	182	1.12×10^{12}	15.5
1.44	6705	6750	−7.13	892	264	1.96×10^{12}	16.5
1.45	6750	6785	−7.34	1045	371	2.26×10^{12}	18.0

2.2. Excitation by the Reynolds stresses

First, we consider excitation by the Reynolds stresses as described by Goldreich et al. (1994). This description, which has also been used by Kumar et al. (1999, hereafter KTZ99), uses a free parameter that has been calibrated on the solar **p**-mode spectrum.

The energy flux per unit frequency due to Reynolds stresses ${\mathcal{F}_{\rm E}}^{\rm R}$ is then

$$ {\mathcal{F}_{\rm E}}^{\rm R}(\ell,\omega) = \frac{\omega^2}{4\pi}\int_{r_c}^{R} {\rm d}r\, \frac{\rho^2}{r^2}\left[\left(\frac{\partial \xi_{\rm r}}{\partial r}\right)^2 + \ell(\ell+1)\left(\frac{\partial \xi_{\rm h}}{\partial r}\right)^2\right] \times \exp\left[-h_\omega^2 \ell(\ell+1)/2r^2\right] \frac{v^3 L^4}{1+(\omega\tau_L)^{15/2}}, \qquad (1) $$

where $\xi_{\rm r}$ and $[\ell(\ell+1)]^{1/2}\xi_{\rm h}$ are the radial and horizontal displacement wave-functions which are normalized to unit energy flux just below the convection zone, v is the mixing length convective velocity, L is the radial size of an energy bearing turbulent eddy, $\tau_L \approx L/v$ is the characteristic convective time, and h_ω is the radial size of the largest eddy at r with characteristic frequency of ω or greater ($h_\omega = L\min\{1,(2\omega\tau_L)^{-3/2}\}$). The gravity waves are evanescent in the convection zone, the region where they are excited. Their wave-functions $\xi_{\rm r}$ and $\xi_{\rm h}$ are thus proportional to $k_{\rm r}^{-1/2}\exp\left(\mathrm{i}\int {\rm d}r\, k_{\rm r}\right)$. The above equation was derived under the assumption that the turbulence spectrum is Kolmogorov. The momentum flux per unit frequency ${\mathcal{F}_J}^{\rm R}$ is then

$$ {\mathcal{F}_J}^{\rm R}(m,\ell,\omega) = \frac{m}{\omega}{\mathcal{F}_{\rm E}}^{\rm R}(\ell,\omega)\,. \qquad (2) $$

The momentum spectra corresponding to the various stellar masses are shown in Fig. 2 where $\mathcal{L}_J = 4\pi r_{\rm cz}^2 \mathcal{F}_J$ is the momentum luminosity; note that some of the lower frequency waves have zero magnitude. This is due to the fact that the corresponding damping is too large to permit them to be waves.

Spectrum characteristics evolve together with the structure of the convection zone which depends on the stellar mass. Low frequency waves disappear when the stellar mass increases. This is related to the fact that the surface convection zone then becomes thinner, leading to a larger thermal diffusivity just below it. This in turn implies stronger damping (see Eq. (6)) and the disappearance of low frequency waves. Furthermore, as stellar mass rises up to about 1.35 $M_\odot$ (i.e., $T_{\rm eff} \sim 6400$ K), so does the flux associated with a given frequency. This is related to the rise of the luminosity with mass, and thus, of the energy in convective motions. For even more massive stars, the flux associated with a given frequency remains about constant, but most low frequency waves are damped too rapidly to exist.

Let us recall that these results are obtained for stellar structures on the ZAMS, and that we have found no significant dependence of the wave spectrum with age on the main sequence; it can thus be considered as constant for the duration of the main sequence.

In this description, waves with frequencies up to N_c (the Brunt-Väisälä frequency at the base of the convective envelope) can be excited. However, the high-frequency waves will have little impact on momentum evolution; indeed, as frequencies increase, filtering by the shear layer (see Sect. 3) becomes less efficient and less differential. Furthermore, damping is so small that it leads to only a small amount of momentum redistribution. Finally, as wave excitation diminishes with frequency, they carry much less momentum overall. These high-frequency waves will form standing waves, the **g**-modes of helio- and astero-seismology.

2.3. Excitation by convective penetration

Greater uncertainties exist on wave generation via convective penetration. The only theoretical estimates that exist have been made by Press (1981) and García López & Spruit (1991), and later used by Zahn et al. (1997). It is the formulation we shall adopt here.

This description is based on the matching of wave pressure fluctuations with those of turbulent convection. Furthermore, it takes into account the combination of turbulent eddies of a given size to produce larger fluctuations. The range of horizontal scales available is thus

$$ 0 < \ell < \ell_u \quad \text{with } \ell_u = \ell_c\left(\frac{\omega}{\omega_c}\right)^{3/2} \qquad (3) $$

where ℓ_c is the spherical harmonic number associated with the largest convective scale and ω_c is the corresponding convective frequency. Turbulence is assumed to follow a Kolmogorov

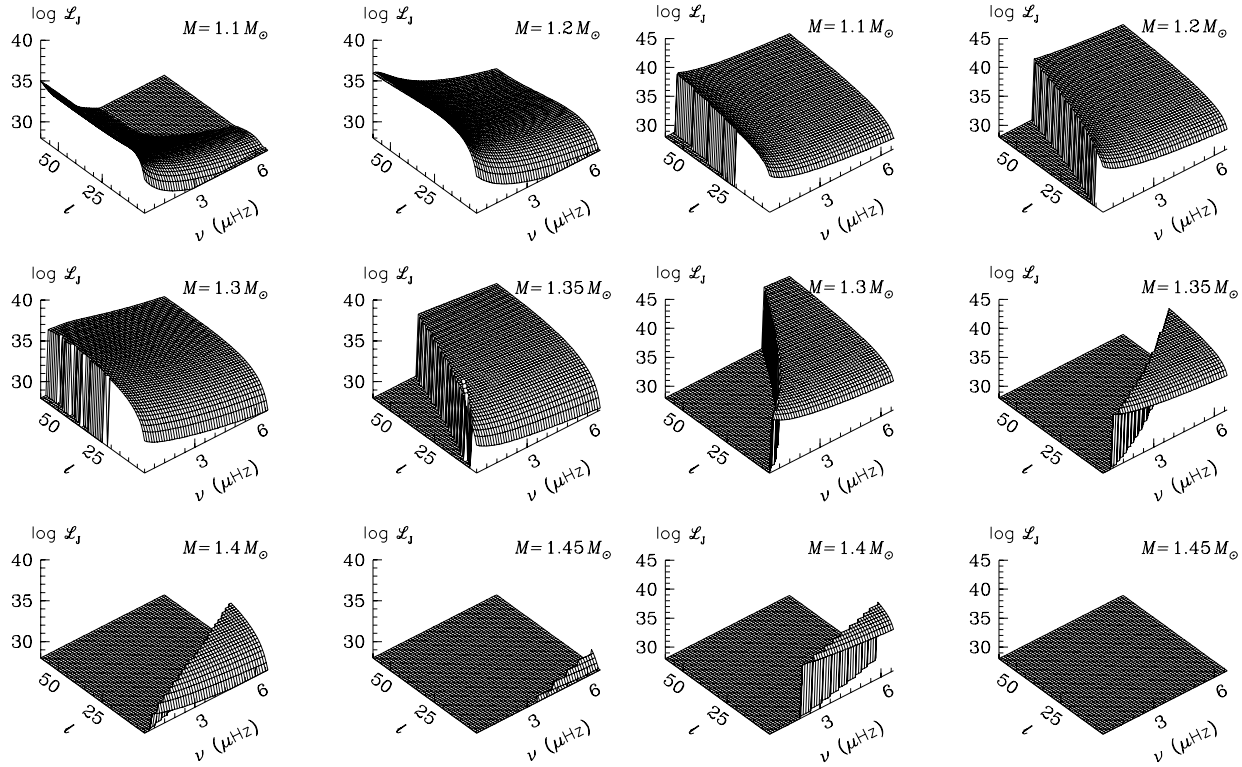

Fig. 2. Momentum spectrum in ℓ and ν for various masses for **(left)** Goldreich, Murray, & Kumar model and **(right)** García López & Spruit model.

spectrum, all frequencies with $\omega \geq \omega_c$ thus being available. The associated energy flux ${\mathcal{F}_E}^P$ is

$$ {\mathcal{F}_E}^P(\ell,\omega) = \frac{\rho v_c^3}{2}\,\frac{\omega_c^3}{\omega^2}\,\frac{\ell}{\ell_c}\,\frac{1}{N}\left(1-\frac{\omega^2}{N^2}\right)^2 \qquad (4) $$

and the corresponding angular momentum flux is still given by Eq. (2).

2.4. A word of caution

Let us stress that the fluxes calculated here are somewhat uncertain, especially in the second case. Indeed, it is well known that the "structure" of convection, which contains e.g. plumes that travel down across the whole convection zone, is not well reproduced by the mixing length model even though the convective velocities are more or less correct (e.g. Hurlburt et al. 1986). However, their differential properties should have the proper dependence, and this will be our focus in the rest of this paper.

3. Formation of a shear layer

3.1. Differential filtering of the waves by a shear layer

As described by several authors (Gough & McIntyre 1998; Ringot 1998, KTZ99, Kim & MacGregor 2001), the most obvious feature of momentum transport by gravity waves is the formation of a double peaked shear layer just below the convection zone (see Fig. 3).

Gough & McIntyre (1998) and Ringot (1998) argued that such a layer would prevent waves from propagating beyond. Indeed, local radiative and viscous damping is greatly dependent on the local frequency and increases when that frequency diminishes (this property leads to the formation of the double peaked shear layer). The local momentum luminosity integrated over the whole spectrum writes

$$ \mathcal{L}_J(r) = \sum_{\sigma,\ell,m} \mathcal{L}_{J\,\ell,m}(r_{zc})\exp\left[-\tau(r,\sigma,\ell)\right]. \qquad (5) $$

The local amplitude $\exp[-\tau(r,\sigma,\ell)]$ depends on the integrated damping due to thermal diffusion K_T and (turbulent) viscosity ν_t

$$ \tau(r,\sigma,\ell) = \qquad (6) $$
$$ [\ell(\ell+1)]^{\frac{3}{2}} \int_r^{r_c} (K_T+\nu_t)\,\frac{N N_T^2}{\sigma^4}\left(\frac{N^2}{N^2-\sigma^2}\right)^{\frac{1}{2}}\frac{\mathrm{d}r}{r^3} $$

where $N^2 = N_T^2 + N_\mu^2$ is the Brunt-Väisälä frequency, N_T^2 is its thermal part and N_μ^2 is due to the mean molecular weight stratification (Zahn et al. 1997).

The prograde peak[2] thus filters prograde waves, while the retrograde peak filters retrograde waves. If the peaks were infinite in height, not a single wave could travel through it. This is however not the case, as the magnitude of the shear layer is self regulated by shear turbulence[3].

[2] The prograde peak corresponds to the layer that rotates more rapidly than the convection zone, while the retrograde peak designates the layer that rotates more slowly.

[3] Baroclinic instabilities could also set in, and would have the same effect.

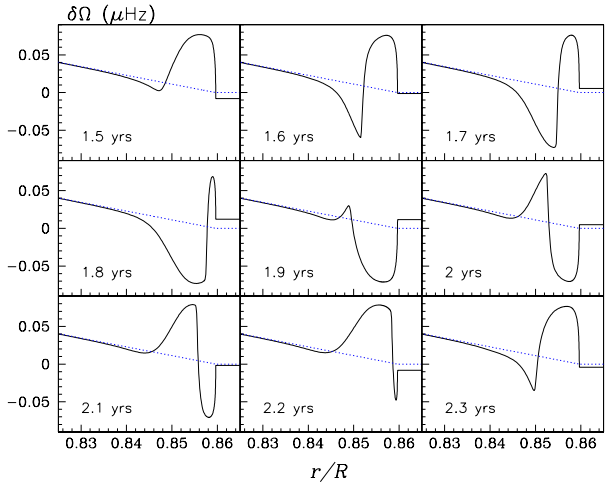

Fig. 3. Oscillating shear layer below the surface convection zone of a 1.2 $M_\odot$ star. The dotted line shows the initial rotation profile. With the surface rotating slower than the core, a prograde shear layer is initially formed, followed by a retrograde one. When the shear becomes too intense, turbulent viscosity acts to merge the prograde layer with the convection zone, leaving behind the retrograde layer. A new prograde layer forms behind, and migrates towards the convection zone when the retrograde layer is absorbed. The cycle then resumes.

As described by TKZ02, if no initial differential rotation is present, the average wave momentum luminosity that traverses the shear layer is null, and there is no net effect on the interior. However, if differential rotation is initially present, as in the case of low mass stars that are braked by a magnetic torque, the average magnitude of the two peaks is not equal; in the case of interest (i.e. with the surface convection zone rotating more slowly than the interior), the prograde peak is always larger, leading to differential filtering that favors the penetration of retrograde waves. These waves are then damped in the whole radiative region that they spin down by depositing negative momentum.

3.2. Dynamics of the shear layer

To study the effect of gravity waves in low mass stars, one must thus be able not only to evaluate the global momentum luminosity in waves, but also the dynamics of the shear layer and the resulting differential filtering. This is addressed here by performing numerical simulations of angular momentum evolution. We study a few cycles and evaluate the resulting net momentum luminosity for various masses and various differential rotations.

Angular momentum evolves under the action of gravity waves and shear turbulence according to

$$\rho \frac{\mathrm{d}}{\mathrm{d}t}\left[r^2\Omega\right] = \frac{1}{r^2}\frac{\partial}{\partial r}\left[\rho \nu_t r^4 \frac{\partial \Omega}{\partial r}\right] - \frac{3}{8\pi}\frac{1}{r^2}\frac{\partial}{\partial r}\mathcal{L}_J(r) \qquad (7)$$

where ρ is the density, Ω the angular velocity and ν_t the turbulent viscosity. The local momentum luminosity $\mathcal{L}_J(r)$ is integrated over the whole wave spectrum. Equation (7) is solved throughout the radiation zone. The upper boundary condition expresses conservation of momentum of the star as a whole, with the convection zone rotating as a solid body. On their way to the core, waves are reflected when their local frequency σ equals the Brunt-Väisälä frequency

$$\sigma(r,m) \equiv \omega - m\left[\Omega(r) - \Omega_\mathrm{c}\right] = N. \qquad (8)$$

Waves then deposit more momentum as they travel back to the surface convection zone. The high-frequency waves of lowest degree considered in this study can be reflected up to 5000 times before they are completely damped; these contribute little to momentum redistribution[4].

Figure 3 shows the oscillation cycle of the shear layer for our 1.2 $M_\odot$ star. Each model (i.e., each stellar mass) has a different characteristic time-scale for this oscillation which depends mainly on the net wave flux in the high degree, low frequency wave. It is thus shortest for masses around 1.2–1.3 $M_\odot$.[5]

4. Momentum extraction

4.1. Fluxes

In all our stellar models, we follow the detailed time evolution of the shear layer according to Eq. (7) over several cycles, for two values of the initial differential rotation (a very small differential rotation of $\delta\Omega = 0.00005\,\mu$Hz over $0.05\,R_*$, and a larger differential rotation $\delta\Omega = 0.05\,\mu$Hz over $0.05\,R_*$). We calculate the net luminosity below the filtering shear layer, at $r = R_{\mathrm{cz}} - 0.03R_*$. Resulting instantaneous and mean luminosities are detailed for the 1.2 $M_\odot$ model in Fig. 4. The change of sign of the instantaneous luminosity illustrates the varying asymmetry of the double peak shear layer. In the case of very small initial differential rotation, the curve is symmetric and the mean luminosity is always close to zero. On the other hand, if the initial differential rotation is large, retrograde waves are favored, as illustrated by the negative mean luminosity. It is this net mean luminosity below the shear layer that gives rise to a net momentum extraction in the interior.

In order to obtain differential filtering, it is important to include several different modes;

- high-ℓ modes, that damp close to the convection zone (see Eq. (6));
- low-ℓ modes, that penetrate deeply.

Furthermore, it is the lowest frequency waves (which undergo the largest amount of differential damping) that give rise to momentum extraction. While wave frequencies range from ~0 to N, for each considered mass, there is a maximum frequency for waves that contribute to differential filtering. That maximum frequency has been determined for each individual mass (see Table 1). In the most massive models considered here, which correspond to stars inside the dip, this maximum frequency is much higher than in lower mass stars. Indeed, as can

[4] As the frequency rises, damping diminishes and standing waves may form.

[5] Let us note that the very different time-scale found in TKZ02 for the Sun is related not only to the smaller flux but also to the reduced number of frequencies and degrees used in order to be able to perform the solar calculation over the required 10^7 time-steps.

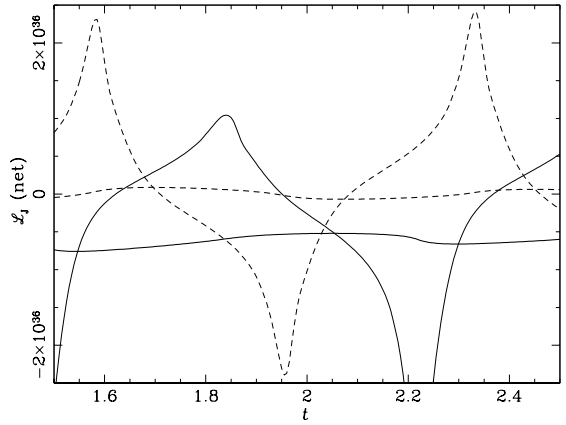

Fig. 4. Net luminosity vs. time (in years) at $0.03\,R_*$ below the surface convection zone. Solid lines correspond to the case of strong initial differential rotation ($\delta\Omega = 0.05\,\mu$Hz over $0.05\,R_*$) and dashed lines to the case of small initial differential rotation ($\delta\Omega = 0.00005\,\mu$Hz over $0.05\,R_*$). Bold lines represent the mean luminosity, thin lines represent the instantaneous luminosity. The curves correspond to a 1.2 $M_\odot$ model. The shear layer oscillation occurs here with a period of ∼1 year.

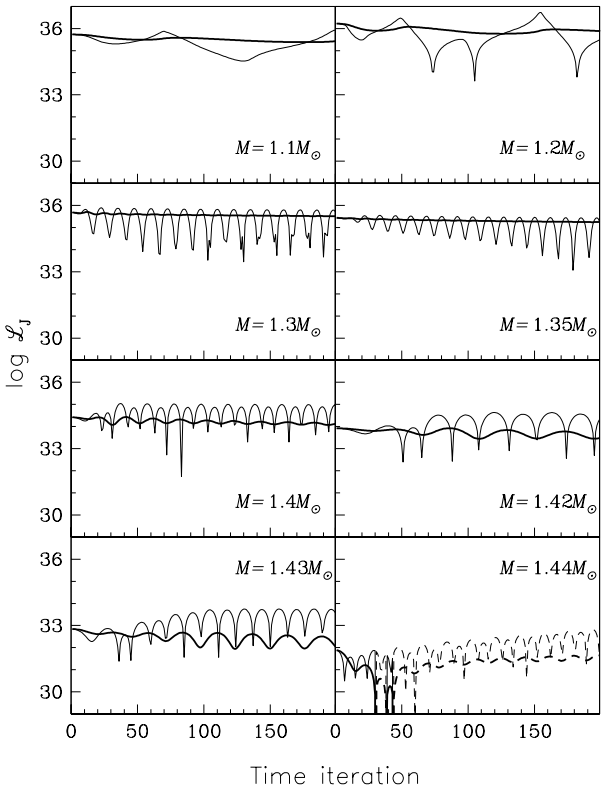

Fig. 5. Net average (bold) and instantaneous (thin) luminosities $0.03\,R_*$ below the surface convection zone after a few cycles for various masses and in the case of "strong" initial differential rotation ($\delta\Omega = 0.05\,\mu$Hz over $0.05\,R_*$). The dashed line corresponds to positives luminosities.

be seen from the wave spectrum (Fig. 2), in those more massive models, high-ℓ modes of low frequency experience too much damping to travel beyond a single vertical wavelength in the vertical. One must thus include higher wave frequencies in order to capture high-ℓ modes that produce the oscillating double peaked shear layer.

The García López & Spruit model for wave excitation by convective penetration leads to the generation of larger frequency waves, leading to a limited amount of extraction. This is especially true for the more massive stars presented in this study and is thus less relevant to our discussion here[6]. For that reason, that model has been ignored in detailed calculations.

The time evolution of the resulting filtering in all stellar masses considered is shown in Fig. 5. The abscissa represents the time iteration, each mass having its own characteristic timescale for oscillation. The results are thus shown in terms of this characteristic time, and not in a real physical time sequence. The net luminosity slightly increases with the stellar mass up to 1.2 $M_\odot$, and then dramatically decreases as one moves to stellar masses inside the Li dip. For the largest mass considered here (1.44 and 1.45 $M_\odot$), the process of differential filtering does not lead to momentum extraction anymore (the net luminosity is actually positive although very small for these stars on the blue side of the dip[7]).

Figure 6 represents the average luminosity after 500 time steps as a function of effective temperature. On the same figure are shown the limits established by TC98 in terms of momentum extraction required in order to consistently understand the Li dip in terms of rotational mixing.

4.2. Coriolis force

In order to fully describe wave transport in rotating stars, we must also take into account the influence of the Coriolis force on waves. Its first order effect is to change the horizontal structure of the modes, confining them closer to the equator. The maximum co-latitude of propagation $\theta_{\rm crit}$ is given by the condition

$$\sigma^2 = 4\Omega^2 \cos^2 \theta_{\rm crit} \tag{9}$$

(KTZ99). For a given rotating velocity, this condition implies that only a fraction

$$\mathcal{S} = \int_{\theta_{\rm crit}}^{\pi/2} \sin\theta \, {\rm d}\theta \tag{10}$$

of the surface will support waves and the corresponding luminosity should be diminished accordingly. Table 2 gives the critical angle for propagation and the corresponding efficiency for a typical frequency of 1 μHz. The rotation velocities used here correspond, for each stellar mass, to the mean velocity observed at the age of the Hyades. Let us note that the fraction of the surface $\mathcal{S}$ varies linearly with ν, and that the whole surface will support waves when $\nu \geq 2\,\nu_{\rm rot}$.

[6] Let us remind that both generating sources are actually additive.

[7] This reverse effect is probably linked to the fact that thermal damping dominates just below the convection zone. Then, the low-ℓ, high frequency waves that are included and that travel back and forth over 100 times, are damped mostly there. However, retrograde waves that have a larger frequency in the interior are less damped there than the prograde waves, leading to an effect opposite to what is observed in other stars.

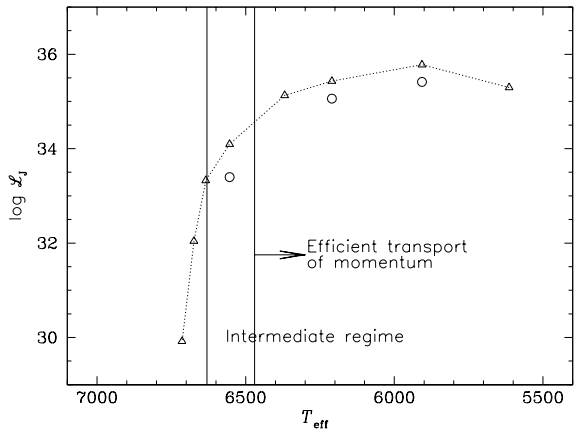

Fig. 6. Net luminosity at $0.03\,R_*$ below the surface convection zone as a function of $T_{\rm eff}$(zams) for an initial differential rotation of $\delta\Omega = 0.05\,\mu$Hz over $0.05\,R_*$. Triangles: without the Coriolis force; circles: including the Coriolis force. The vertical lines correspond to the requirement of angular momentum efficiency as described by TC98 (they correspond to the horizontal lines of their Fig. 2).

Table 2. Effect of the Coriolis force.

M_* ($M_\odot$)	$T_{\rm eff}$ (K)	$\langle v\rangle_{\rm Hyades}$ (km s^{-1})	$\nu_{\rm rot}$ (μHz)	$\nu_{\rm wave}$ (μHz)	$\theta_{\rm crit}$	$\mathcal{S}$ (%)
1.1	5640	8	1.65	1	72.4	30.2
1.2	5950	10	1.90	1	74.7	26.3
1.3	6260	20	3.50	1	81.8	14.3
1.35	6420	30	5.05	1	84.3	9.9
1.4	6595	50	8.10	1	86.5	6.2
1.45	6790	75	11.5	1	87.5	4.3

Exact calculations can be made by reducing the wave luminosity corresponding to each frequency by the proper coefficient. This has been done for 3 models (1.2, 1.3 and 1.4 $M_\odot$). The amplitude of low frequency waves (that dominate the formation of the shear layer) being reduced, including the Coriolis force leads to a somewhat smaller double peaked shear layer, that oscillates on a slightly longer period. Furthermore, differential filtering corresponding to momentum extraction is also dominated by rather low frequency waves. This leads to a smaller efficiency of momentum extraction by waves (see Fig. 6). However, the overall mass dependence is not affected.

5. Discussion

Several abundance anomalies are best explained in terms of large-scale mixing. As a natural physical parameter (beyond mass, chemical composition and age), rotation is an important factor in understanding various features which are not predicted from classical stellar models (see Maeder & Meynet 2000 for details). Furthermore, if one is to built a consistent model of rotational mixing, it has to apply to all stars.

Recent improvements of the description of the Eddington-Sweet meridional circulation by Zahn (1992) and Maeder & Zahn (1998) have been applied to several kinds of stars. These studies show that, with the same free parameters, it is possible to explain abundance anomalies in B (Talon et al. 1997) and O stars (Maeder & Meynet 2000) as well as the blue side of the Li dip (TC98, PTCF03) and Li anomalies in sub-giants (Charbonnel & Talon 1999).

However, in order to understand the helioseismic rotation profile, some extra mechanism for momentum transport is required in low mass stars (Matias & Zahn 1998). TC98 argued that, for rotational mixing to be responsible for the Li dip, this mechanism has to become efficient at an effective temperature around ~6500−6600 K, i.e., in a region where the stellar convective envelope becomes substantial. If the same description is to be applied to all stars, there must be some physical reason for the lack of efficiency of this mechanism in hotter stars. The goal of this paper was to establish whether gravity waves do have the proper effective temperature dependence.

The calculations we performed here show that the built up of a double peaked shear layer allowing differential filtering of the waves is possible in low-mass main sequence stars up to an effective temperature of ~6700 K. The net momentum luminosity below the shear layer increases with stellar mass up to 1.2 $M_\odot$ (i.e., $T_{\rm eff} \sim 5900-5950$ K); it then drops in hotter stars, even becoming slightly positive for stars more massive than ~1.44 $M_\odot$ (i.e., $T_{\rm eff} > 6700$ K). While the quantitative results shown here are based on the excitation model by Goldreich et al. (1994), the García López & Spruit (1991) model would lead to an even stronger decrease in efficiency. Indeed, as can be seen in Fig. 2, in the more massive models, there are simply no low frequency waves, implying an even more abrupt decrease in the efficiency of differential filtering.

Let us discuss a final issue. As can be seen from Fig. 1, the dispersion in lithium abundances is somewhat larger on the cold side of the dip ($T_{\rm eff} \sim 6000-6500$ K) than in cooler stars. A very straightworward explanation of this arises within our framework. As we have shown indeed, for a given stellar mass a higher rotation velocity implies a stronger reduction of the net momentum luminosity in waves due to the Coriolis force. As a consequence, the efficiency of angular momentum extraction by the waves is somewhat lower within faster rotators, leading to a larger efficiency of the hydrodynamical processes, and thus to stronger Li destruction. In this context, the larger lithium dispersion measured in stars laying immediatly on the right of the dip can be interpreted as a consequence of the larger dispersion in rotational velocities that these stars do exhibit in comparison with the less massive ones (Gaigé 1993). Detailed calculations would have to be performed to check whether this effect could be large enough to explain the observed dispersion.

All our results clearly indicate that momentum transport by gravity waves has the proper mass dependence to be the required process in low-mass main sequence stars on the cold side of the Li dip.

Note that a similar mass dependence is not expected if momentum transport is dominated by magnetic fields. There is another test which could permit to differentiate the magnitude of transport by magnetic field compared to transport by waves which applies to the Sun. Certain early helioseismic inversions (Elsworth et al. 1995; Corbard et al. 1997) suggested that the central region of the Sun (below ~$0.4\,R_\odot$) could rotate somewhat slower than the rest of the radiative region. These results seem to be confirmed by recent SOHO data (Couvidat et al. 2003). TKZ02 explained how such a feature could be produced

by gravity waves. Both arguments favor momentum transport by gravity waves with respect to magnetic field.

We are now in a position to present a coherent picture of rotational mixing in main sequence stars of all masses:
On the hot side of the Li dip and in more massive stars, the transport of angular momentum and of chemicals by meridional circulation and shear instabilities do explain the Li as well as the He and CNO patterns. In lower mass stars, gravity waves dominate the transport of angular momentum, thereby reducing the magnitude of meridional circulation and shears and shaping the Li pattern on the cold side of the dip. Within this framework, we thus predict that Pop I main sequence stars with initial masses lower than $\sim$1.4 $M_{\odot}$ must be quasi-solid body rotators, as the Sun is.

Acknowledgements. We acknowledge financial support from the French Programme National de Physique Stellaire (PNPS). We thank the Réseau québécois de calcul de haute performance (RQCHP) and the Centre informatique national de l'enseignement supérieur (CINES) for useful computational resources.

References

Balachandran, S. 1995, ApJ, 446, 203
Balmforth, N. J. 1992, MNRAS, 255, 639
Barnes, G., Charbonneau, P., & MacGregor, K. B. 1999, ApJ, 511, 466
Boesgaard, A. M., & Tripicco, M. J. 1986, ApJ, 302, L49
Boesgaard, A. M. 1987, PASP, 99, 1067
Chaboyer, B., Demarque, P., Guenther, D. B., & Pinsonneault M. H. 1995, ApJ, 446, 435
Charbonneau, P., & MacGregor, K. B. 1993, ApJ, 417, 762
Charbonnel, C., & Talon, S. 1999, A&A, 351, 635
Corbard, T., Berthomieu, G., Morel, P., et al. 1997, A&A, 324, 298
Couvidat, S., Turck-Chièze, S., Garcia, R. A., & Corbard, T. 2003, in 3D Stellar Structure Workshop, ASP Conf. Ser., ed. R. Cavallo, S. Keller, & S. Turcotte
Elsworth, Y., Howe, R., Isaak, G. R., et al. 1995, Nature, 376, 669
Gaigé, Y. 1993, A&A, 269, 267
García López, R. J., & Spruit, H. C. 1991, ApJ, 377, 268
Gies, D. R., & Lambert, D. L. 1992, ApJ, 387, 673
Goldreich, P., & Kumar, P. 1990, ApJ, 363, 694
Goldreich, P., Murray, N., & Kumar, P. 1994, ApJ, 424, 466
Gough, D. O., & McIntyre, M. E. 1998, Nature, 394, 755
Herrero, A., Kudritzki, R. P., Vilchez J. M., et al. 1992, A&A, 261, 209
Hurlburt, N. E., Toomre, J., & Massaguer, J. M. 1986, ApJ, 311, 563
Hurlburt, N. E., Toomre, J., Massaguer, J. M., & Zahn, J.-P. 1994, ApJ, 421, 245
Kim, Eun-jin, & MacGregor, K. B. 2001, ApJ, 556, L117
Kiraga, M., Różyczka, M., Stepien, K., Jahn, K., & Muthsam, H. 2000, Acta Astron., 50, 93
Kumar, P., & Quataert, E. J. 1997, ApJ, 475, L143
Kumar, P., Talon, S., Zahn, J.-P. 1999, ApJ, 520, 859 (KTZ)
Lennon, D. J., Becker, & ST, Butler K., et al. 1991, A&A 252, 498
Maeder, A. 1995, A&A, 299, 84
Maeder, A., & Meynet, G. 2000, ARA&A, 38, 143
Maeder, A., & Zahn, J. P. 1998, A&A, 334, 1000
Matias, J., & Zahn, J.-P. 1998, in Sounding solar and stellar interiors, IAU Symp. 181, poster volume, ed. J. Provost & F. X. Schmider
Meylan, G., & Maeder, A. 1982, A&A, 108, 148
Nordlund, A., Stein, R. F., & Brandenburg, A. 1996, Bull. Astron. Soc. of India 24, 261
Palacios, A., Talon, S., Charbonnel, C., & Forestini, M. 2003, A&A, 399, 603 (PTCF03)
Press, W. H. 1981, ApJ, 245, 286
Ringot, O. 1998, A&A, 335, 89
Schatzman, E. 1993, A&A, 279, 431
Talon, S. 2003, in Stellar Rotation, IAU Symp. 215, ed. A. Maeder, & P. Eenens
Talon, S., & Charbonnel, C. 1998, A&A, 335, 959 (TC98)
Talon, S., Kumar, P., & Zahn J.-P. 2002, ApJ, 574, L175 (TKZ02)
Talon, S., & Zahn, J.-P. 1997, A&A, 317, 749
Talon, S., Zahn, J. P., Maeder, A., & Meynet, G. 1997, A&A, 322, 209
Takeda, Y., Kawanomoto, S., Takada-Hidai, M., & Sadakane, K. 1998, PASJ, 50, 509
Townsend, A. A. 1958, J. Fluid Mech., 4, 361
Varenne, O., & Monier, R. 1999, A&A, 351, 247
Venn, K. 1999, ApJ, 518, 405
Wallerstein, G., Herbig, G. H., & Conti, P. S. 1965, ApJ, 141, 610
Zahn, J. P. 1992, A&A, 265, 115
Zahn, J.-P., Talon, S., & Matias, J. 1997, A&A, 322, 320